Linking extreme precipitation in Southeast Asia to equatorial waves

Article

Ferrett, S. ORCID: https://orcid.org/0000-0003-4726-847X, Yang, G.-Y. ORCID: https://orcid.org/0000-0001-7450-3477, Woolnough, S. J. ORCID: https://orcid.org/0000-0003-0500-8514, Methven, J. ORCID: https://orcid.org/0000-0002-7636-6872, Hodges, K. ORCID: https://orcid.org/0000-0003-0894-229X and Holloway, C. E. ORCID: https://orcid.org/0000-0001-9903-8989 (2020) Linking extreme precipitation in Southeast Asia to equatorial waves. Quarterly Journal of the Royal Meteorological Society, 146 (727). pp. 665-684. ISSN 1477-870X doi: https://doi.org/10.1002/qj.3699 Available at https://centaur.reading.ac.uk/87464/

It is advisable to refer to the publisher's version if you intend to cite from the work. See Guidance on citing.

To link to this article DOI: http://dx.doi.org/10.1002/qj.3699

www.reading.ac.uk/centaur

CentAUR

Central Archive at the University of Reading

Reading's research outputs online

RESEARCH ARTICLE

Linking extreme precipitation in Southeast Asia to equatorial waves

Samantha Ferrett[1] | Gui-Ying Yang[1] | Steven J. Woolnough[1] | John Methven[2] | Kevin Hodges[1] | Christopher E. Holloway[2]

[1]National Centre of Atmospheric Science, Department of Meteorology, University of Reading, Reading, UK

[2]Department of Meteorology, University of Reading, Reading, UK

Correspondence
S. Ferrett, National Centre of Atmospheric Science, Department of Meteorology, University of Reading, Earley Gate, PO Box 243, Reading RG6 6BB, UK.
Email: s.j.ferrett@reading.ac.uk

Abstract

Equatorially trapped waves, such as Kelvin Waves, Equatorial Rossby Waves and Westward-moving Mixed Rossby–Gravity (WMRG) Waves, play a major role in organising tropical convection on synoptic to sub-seasonal time-scales. These waves have the potential to provide an important source of predictability for high-impact weather in Southeast (SE) Asia and the Tropics more widely. To aid understanding of the role played in high-impact weather by such waves, the observed statistical relationship between identified equatorial waves and heavy rainfall in SE Asia is examined for the period 1998–2016. Increases in the amount of precipitation and the likelihood of extreme precipitation in SE Asia are linked to all three types of waves that are included in analysis; Kelvin, equatorial Rossby and WMRG waves. There is both increased mean rainfall and increased probability of occurrence of heavy rainfall on days when high-amplitude waves propagate over SE Asia. In particular, heavy precipitation can be up to three times more likely in regions of SE Asia during equatorial waves, including Malaysia, Indonesia and the Philippines. Kelvin waves have a large influence on heavy rainfall over Indonesia, WMRG and Kelvin waves impact Malaysia rainfall, and equatorial Rossby and WMRG waves are linked to increased rainfall over the Philippines. Based on this study it can be concluded that the probability of extreme precipitation in this region is dependent on equatorial wave activity. Therefore, the skill in probabilistic prediction of extreme precipitation in SE Asia would be expected to be conditional on the skill in equatorial wave prediction, and the modelled relationship between equatorial waves and convection.

KEYWORDS

Kelvin, precipitation, Rossby, Southeast Asia, tropical waves, westward mixed Rossby–gravity

1 | INTRODUCTION

Southeast (SE) Asia is prone to high-impact weather, and is often subject to flooding and landslides as a result of heavy rainfall. Moreover, the seasonal cycle of rainfall in different regions of SE Asia behaves differently (Hamada *et al.*, 2002). Rainfall in Peninsular Malaysia and Indonesia tends to occur more in boreal winter, as a result of the Asian winter monsoon (e.g. Chang *et al.*, 2005a; 2006), as indicated in Figure 1. Both mean and heavy rainfall during boreal winter are largest over the east coast of Peninsular Malaysia, in regions of Sumatra and Java, along the northwest coast of Borneo, and on the east coast of the Philippines (Figure 1a,e). During boreal summer, rainfall is heavier in the Northern Hemisphere, with more precipitation occurring in the northeast of the Bay of Bengal and along the west coast of the Philippines, as a result of the Asian summer monsoon (Figure 1c,f). Climatological heavy rainfall, defined here as rainfall exceeding the 95% percentile, follows similar spatial patterns and seasonal cycle as that of mean rainfall (Figure 1e,f). Global models used for numerical weather prediction have been known to fail to accurately capture Maritime Continent convection (e.g. Love *et al.*, 2011; Birch *et al.*, 2016; Johnson *et al.*, 2016), limiting predictions of high-impact weather in the region.

Tropical convective systems are organised by modes of variability on varying space and time scales, such as the Madden–Julian Oscillation (MJO: Madden and Julian, 1971; 1972; 1994) and equatorially trapped waves (Matsuno, 1966). In SE Asia, enhanced precipitation has been linked to a variety of weather systems, such as the Borneo vortex, cold surges, tropical cyclones, and the MJO (Chang *et al.*, 2005b; Juneng *et al.*, 2007; Tangang *et al.*, 2008). Moreover, these systems can interact with one another, further increasing extreme precipitation associated with them (Chang *et al.*, 2005b; 2016). In particular, it has been noted that the MJO can modulate the occurrence of cold surge events, tropical cyclogenesis and the Borneo vortex (Liebmann *et al.*, 1994; Chang *et al.*, 2005b; Li *et al.*, 2012; Lim *et al.*, 2017), as well as impact the resulting extreme rainfall (Chang *et al.*, 2016; Lim *et al.*, 2017). Similarly, Xavier *et al.* (2014) established a statistical link between extreme SE Asia rainfall and the MJO. However, such a link with equatorial waves, existing on shorter time-scales and smaller spatial scales, is yet to be established.

Theoretical structures of equatorial waves were described by Matsuno (1966) as solutions to the shallow-water equations and have since been identified in observations (Wheeler *et al.*, 2000; Yang *et al.*, 2003; Roundy and Frank, 2004; Tsuda *et al.*, 2006; Kiladis *et al.*, 2009; Masunaga, 2009). Equatorial wave modes, such as the Kelvin, mixed Rossby–gravity and equatorial Rossby

waves, are known to play a large role in tropical weather via their coupling to tropical convection (Takayabu, 1994; Wheeler and Kiladis, 1999; Wheeler *et al.*, 2000; Yang *et al.*, 2003; Murata *et al.*, 2006; Kiladis *et al.*, 2009; Kim and Alexander, 2013; Schlueter *et al.*, 2019). Therefore it is essential that global circulation models fully capture their observed behaviour, as a matter of importance for tropical high-impact weather prediction. Numerous studies have established the difficulties in accurately predicting tropical waves and associated weather (e.g. Yang *et al.*, 2009; Huang *et al.*, 2013; Ying and Zhang, 2017).

While previous studies have described the link between equatorial waves and tropical convection (e.g. Straub and Kiladis, 2001; Yang *et al.*, 2003; Kiladis *et al.*, 2009) and their link to extreme rainfall in India and Vietnam (Van Der Linden *et al.*, 2016; Subudhi and Landu, 2019), the role high-amplitude equatorial waves play in rainfall extremes in SE Asia is less well defined. To improve predictability of high-impact weather in the Tropics, it is of great importance that the observed relationship between equatorial waves is fully understood, in order to be captured by global forecast models. With this aim, this study aims to characterise the observed statistical relationship between SE Asia rainfall and high-amplitude Kelvin, equatorial Rossby and mixed Rossby–gravity waves, and also focuses on the link between equatorial waves and extreme precipitation in SE Asia. We focus on these three waves as these are the gravest wave modes and are on spatial and time-scales most relevant to daily rainfall near the Equator. This study follows the methodology described in Yang *et al.* (2003) to identify waves based on their dynamical structure. This has the advantage over other methods as no information about precipitation is used to identify the wave, therefore any linkage between precipitation and equatorial waves is not a result of the identification method.

Section 2 outlines the methods used to identify equatorial waves and to examine the observed relationship between equatorial waves and high-impact rainfall in SE Asia. Results of statistical analysis of the relationship between equatorial waves and SE Asia rainfall are given in Section 3, including the link between waves and the likelihood of heavy rainfall. Section 4 provides a summary and discussion of the findings of the study.

2 | DATA AND METHODS

2.1 | Equatorial wave datasets

Equatorially trapped waves are obtained as solutions to the adiabatic, frictionless equations of motion on
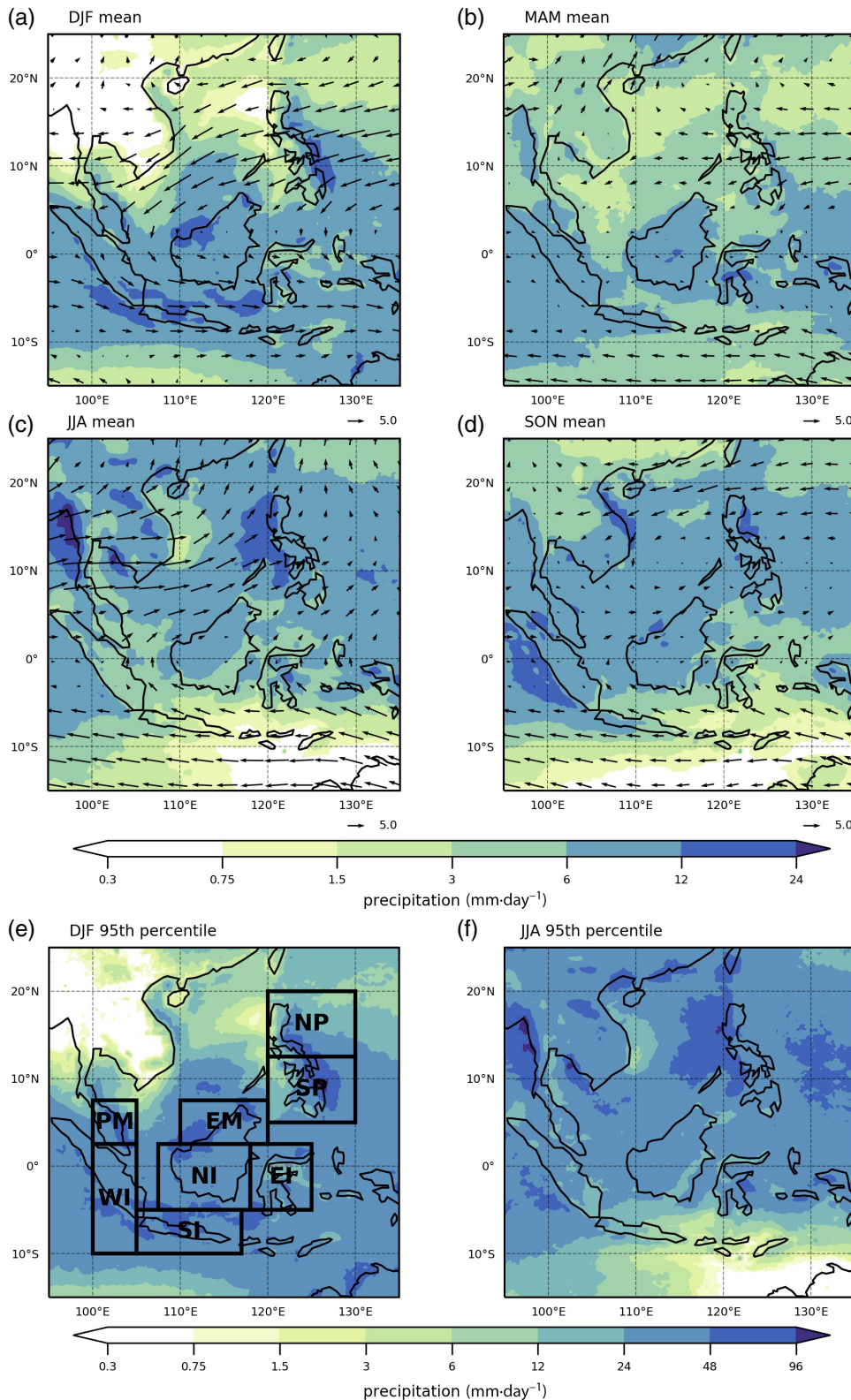
FIGURE 1 Seasonal mean of 1998–2016 TRMM precipitation for (a) December–February, (b) March–May, (c) June–August, and (d) September–November. Seasonal 95th percentile of daily precipitation calculated at each grid point for (e) DJF and (f) JJA. Vectors in (a–d) are the seasonal mean ERA-Interim 850 hPa winds for the same time period. Boxed regions of interest for Malaysia (PM and EM), Indonesia (NI, EI, SI and WI) and the Philippines (NP and SP) are shown in (e). Note that analysis using these regions only uses land points

an equatorial β-plane, linearized about a state of rest and separation of the vertical structure from that in the horizontal (Matsuno, 1966; Gill, 1980). The horizontal and temporal behaviour of horizontal winds (u, v) and geopotential height (Φ) satisfy the linearized shallow-water equations with gravity-wave speed c_e, the separation constant from the vertical structure equation that can also satisfy relevant surface and upper boundary conditions. This is possible only for discrete values of the separation constant, c_e. c_e increases with static stability

and reduces with vertical wave number. According to Gill (1980) the meridional (y) structures of equatorial waves can be described by parabolic cylinder functions. These functions form a complete and orthogonal basis. The theoretical horizontal structures of some of the gravest equatorial waves are shown in Figure 2.

There is the Kelvin wave solution with zero v; the Kelvin wave is eastward moving. Other solutions with non-zero v are the $n = 0$ mode, the mixed Rossby–gravity (MRG) wave, which has both eastward- (EMRG) and westward-moving (WMRG) solutions. For $n = 1$ and higher there are low-frequency westward-moving equatorial Rossby waves (e.g. R1) and both eastward and high-frequency westward-moving gravity-wave solutions.

Many previous studies have used a method to identify equatorial waves by isolating disturbances in zonal wave number and frequency domains confined by theoretical dispersion curves for a variety of specified equivalent depths for the waves (e.g. Wheeler and Kiladis, 1999; Wheeler et al., 2000). However, although the separation of the vertical and horizontal structures is possible for a resting atmosphere or uniform zonal flow, in general the separation of variables for observed atmospheric disturbances is not possible due to a number of factors such as: atmosphere being far from resting, shear in the zonal flow, the complicated space–time dependence of the ambient state, the feedback from convective heating organised by the wave, nonlinearities, non-uniform damping, and the lack of a rigid lid. Therefore analysis in terms of vertical modes and horizontal wave structures is not strictly valid. All these factors can be expected to lead to distortion of the theoretical dispersion curves; at the very least there can be an expectation of some Doppler shifting (Dias and Kiladis, 2014), and perhaps invalidity of the modal separation in the vertical and hence the concept of equivalent depth. Consequently, different equatorial modes may not, in reality, be well separated in the frequency and zonal wave-number domain. For example, the WMRG and meridional mode number $n = 1$ Rossby (R1) waves, which are often in a very close zonal wave-number–frequency domain, can sometimes merge together, as shown in Yang et al. (2007c). Also a strong basic flow in the Tropics would lead waves to be Doppler-shifted to move to the opposed direction as expected in the theory, for example intrinsic westward-moving WMRG and R1 waves can be Doppler-shifted to move eastward in the upper
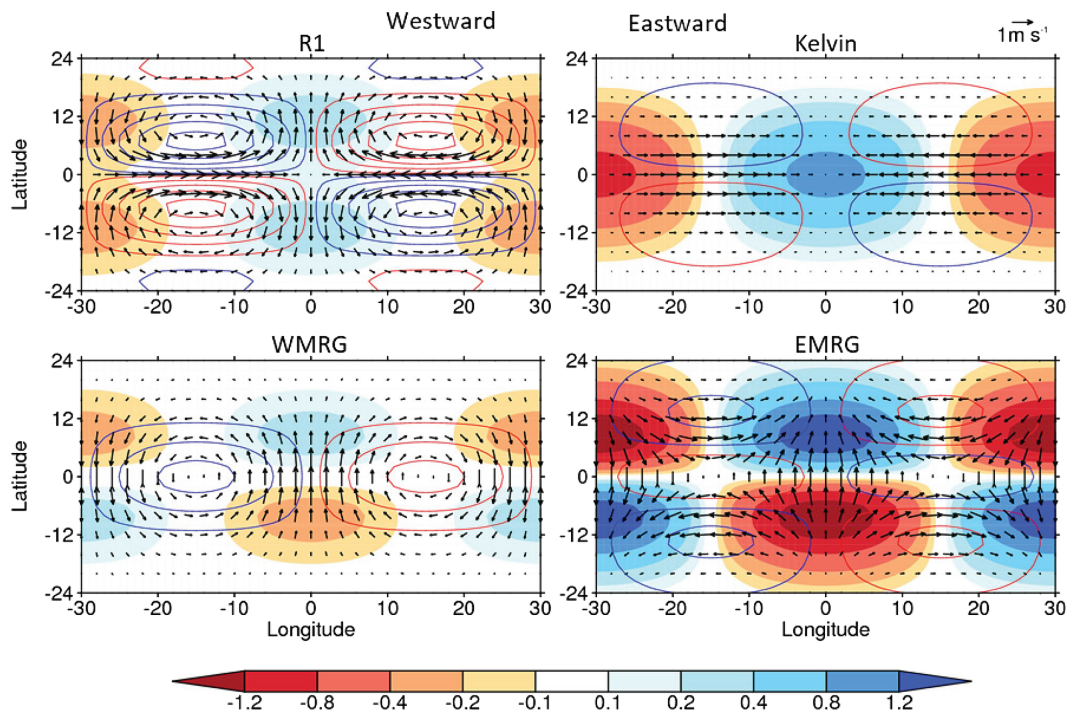
FIGURE 2 The theoretical horizontal structures of some of gravest equatorial wave modes in the resting atmosphere. The Kelvin wave, the $n = 0$ westward-moving mixed Rossby–gravity (WMRG) and the eastward-moving mixed Rossby–gravity (EMRG), the $n = 1$ westward-moving Rossby (R1) waves. The meridional trapping scale $y0$ has been taken to be 6° and the zonal wave number $k = 6$. Vectors indicate horizontal wind. Filled contours indicate divergence ($10^{-6} \cdot s^{-1}$) with convergence set to be positive. Colour contours lines are vorticity ($10^{-6} \cdot s^{-1}$) with blue lines for positive vorticity and red lines for negative vorticity; the contour interval is 0.6 starting from ± 0.2. The maximum zonal wind for the Kelvin wave and the maximum meridional wind for the $n = 0$ MRG are set to be $1 \, m \cdot s^{-1}$, and maximum meridional wind for the $n = 1$ Rossby (R1) wave is set to be $\sim 0.86 \, m \cdot s^{-1}$

tropospheric westerly ducts (Yang and Hoskins, 2016). Hence in Yang *et al.* (2003), a less constraining methodology for identifying equatorial waves in observational data was developed.

In the methodology, it was not assumed that the linear adiabatic theory for equatorial waves on a resting atmosphere is directly applicable; in particular, the dispersion relation and vertical structure are not imposed, and hence the methodology is not limited to a prescribed space–time spectral filter but accounts for Doppler shift automatically. Potential equatorial waves are identified by projecting the dynamical fields in the Tropics at each pressure level onto a set of horizontal structure basic functions described by parabolic cylinder functions in y and sinusoidal variation in x.

This level-by-level projection technique has been successfully employed in a wide range of studies to investigate the horizontal and vertical structures of convectively coupled equatorial waves both in observations (e.g. Yang *et al.*, 2007a; 2007b; 2007c) and models (Yang *et al.*, 2009), the variation of equatorial waves in different phases of QBO (Yang *et al.*, 2011; 2012), the influence of ENSO on equatorial waves and tropical convection (Yang and Hoskins, 2013; 2016), and connection between African Easterly waves and equatorial waves (Yang *et al.*, 2018). Full details of the analysis method are described in the study of Yang *et al.* (2018).

2.2 | Tropical cyclone identification

Two datasets are used to identify tropical cyclones that occur in the vicinity of high-amplitude waves. The International Best Track Archive for Climate Stewardship (IBTrACS: Knapp *et al.*, 2010) combines tropical cyclone track data from 12 different agencies and historical databases to produce a database of historical tracks. We use the World Meteorological Organisation (WMO) subset. The WMO subset are the observations obtained by the WMO-sanctioned agency for the region, in this case the Japan Meteorological Agency (JMA). The study of Barcikowska *et al.* (2012) found JMA to be more consistent in the information used to determine location and intensities than those of the Joint Typhoon Warning Center (JTWC), and better than JTWC when compared with scatterometer data.

The second dataset identifies tropical cyclone tracks in ERA-Interim. This is done using an objective feature tracking method that tracks all tropical systems through their full life cycles and then matches the tracks against those of IBTrACS to identify the identically same tropical cyclones (TCs); a full description of the tracking and matching methodology is given in Hodges *et al.* (2017).

This has the benefit of identifying more of the TC life cycle, such as the part before the system is declared a TC and also after it is no longer followed by the operational observing centres. Thus the TC tracks identified in the reanalysis are typically longer than those in IBTrACS. Both datasets are used to produce Table 1; only the second is used to divide high-amplitude wave days into TC and non-TC days in Section 3.2.3. In Table 1 a tropical cyclone is defined as in the vicinity of a high-amplitude wave if it occurs within 10° of the longitude bounds used for the wave and between latitude 5 and 25°N. In Section 3.2.3 a tropical cyclone is counted if it is in the longitude range 110–135°E, since waves at 120–125°E are most strongly linked to the Philippines.

2.3 | Rainfall and wave analysis

The equatorial wave datasets (described in Section 2.1) for Kelvin, equatorial Rossby (R1) and WMRG waves (1997–2016) are used to examine the relationship between equatorial wave activity and rainfall over SE Asia. Daily mean Tropical Rainfall Measuring Mission (TRMM) 3B42 version 7 research rainfall (Huffman *et al.*, 2007; Huffman et al., 2010) is used for rainfall analysis at $0.25° \times 0.25°$ spatial resolution for 1998–2016. The product combines satellite estimates and precipitation from rain-gauges where data are available. Zonal and meridional winds and geopotential height used for the wave dataset and other analyses are taken from the European Centre for Medium-range Weather Forecasts (ECMWF) global reanalysis ERA-Interim (Dee *et al.*, 2011).

A metric of wave activity is obtained using average convergence (for Kelvin and WMRG waves) or vorticity (for R1 waves) of the 850 hPa wind associated with the waves over a selected longitude range and a latitude appropriate for the wave structure. Vorticity is chosen for the R1 wave since the wave is dominated by vorticity rather than convergence; the structure indicates vortices either side of the Equator (Figure 2). This is captured better in composite analysis using vorticity to identify high-amplitude waves, though precipitation responses are associated with the wave when using convergence to identify high-amplitude R1 waves also (not shown in figures). WMRG waves also have a rotational component. However, both compositing by WMRG convergence and by WMRG vorticity find that the changes in precipitation coincide with where the composite convergence is located, as opposed to the location of cyclonic or anticyclonic activity. Therefore, WMRG convergence is chosen to be used for composites. Here, wave activity at longitude ranges 90–95°E, 100–105°E, 110–115°E and 120–125°E is considered. The longitude width of 5° is selected to best capture regions of interest in

TABLE 1 Summary of number of days in each season with a high-amplitude R1 or WMRG wave, a high-amplitude wave and a tropical cyclone using tracked tropical cyclone historical dataset (wave + TC), a high-amplitude wave and a tropical cyclone using IBTrACS (wave + IBTrACS), and both R1 and WMRG high-amplitude waves (R1 + WMRG), at various longitude ranges (°E)

Longitude range	DJF				JJA			
	90–95	100–105	110–115	120–125	90–95	100–105	110–115	120–125
R1	72	84	104	108	131	125	101	112
wave + TC	11 (15%)	21 (25%)	46 (44%)	41 (38%)	14 (11%)	37 (24%)	70 (69%)	100 (89%)
wave + IBTrACS	7 (10%)	12 (14%)	42 (40%)	45 (42%)	14 (11%)	29 (23%)	65 (64%)	89 (79%)
WMRG	100	148	97	109	128	93	105	108
wave + TC	9 (9%)	20 (14%)	25 (26%)	32 (29%)	13 (10%)	45 (48%)	81 (77%)	93 (86%)
wave + IBTrACS	10 (10%)	10 (7%)	20 (21%)	26 (24%)	4 (3%)	40 (43%)	77 (73%)	90 (83%)
R1+WMRG	7	12	11	19	17	17	27	19

Note. Percentages of the total number of R1 or WMRG wave days are also given. Tropical cyclones are counted if they are within 10° of the longitude bounds used for the wave and between latitude 5 and 25°N.

SE Asia, such as Peninsular Malaysia and the Philippines. The selected latitude varies depending on the wave, and is chosen to capture the peak of wave activity about the Equator; 0° for Kelvin wave, 8°N for R1 wave, and 10°N for WMRG wave. However, the meridional structures of the waves are defined by the parabolic cylinder functions and so results are independent of this choice. Using this metric, days with high-amplitude wave activity in the selected longitude region are classified as those in which convergence or vorticity associated with the wave exceeds the 95th percentile of 1998–2016. For WMRG waves the meridional structure is asymmetric about the Equator and so it can be important for regions such as Java to examine both the 95th and the fifth percentile, in other words the days when there is high-amplitude convergence in the Northern Hemisphere (we label these days WMRG +ve in figures) and the days when there is high-amplitude wave convergence in the Southern Hemisphere (labelled WMRG –ve in figures).

Line contours in Figure 4 show the composite wave convergence or vorticity at the specified latitude listed above preceding and following high-amplitude wave days over 100–105°E. The identified waves propagate at appropriate speeds and have group velocities consistent with what would be expected from theory and has been observed.

Identifying waves in this way allows statistical analysis of observed precipitation during high-amplitude wave days. Two metrics of precipitation are used to assess the influence of equatorial waves on precipitation. The first is the seasonal composite anomaly of daily precipitation on high-amplitude wave days from the climatological seasonal mean. The second is a measure based on the change in frequency of heavy precipitation and can be thought of as the change in the likelihood of heavy precipitation.

This is calculated based on the probability of precipitation exceeding a precipitation threshold on days when a high-amplitude wave occurs. The threshold is calculated as the 95th percentile of precipitation of all days in the season during the time period 1998–2016.

3 | RESULTS

3.1 | Equatorial waves and SE Asia rainfall

3.1.1 | Mean SE Asia rainfall

Seasonal mean rainfall is increased, relative to the climatological seasonal mean for 1998–2016 (see Figure 1 and Section 1 for description), on days with high-amplitude wave activity, and can be associated with the propagation of the waves over SE Asia. Figure 3 shows composites of the anomalies of seasonally averaged precipitation, from the respective climatological seasonal means, at various latitudes in the days preceding and following a high-amplitude wave at 100–105°E, labelled day 0 in Figure 3. The Kelvin wave propagates eastward; there is composite wave low-level convergence around 80°E two to 4 days preceding day 0, as indicated by the solid line contours in Figure 3a,d. This is accompanied by significant positive rainfall anomalies along the Equator. The wave convergence propagates eastward and is visible around 125°E up to 4 days following day 0. The rainfall anomalies propagate eastward with the wave convergence. Rainfall anomalies are strongest over the ocean explaining why the strength of the rainfall anomalies varies with longitude in Figure 3, seemingly independent of the strength of the wave convergence. In the days following wave

convergence and increased rainfall there is suppressed rainfall coincident with wave divergence (dashed line contours in Figure 3).

Similar relationships are shown between rainfall and wave activity for the westward propagating WMRG and R1 waves (Figure 3b,c,e,f). However, the relationship between the R1 wave and precipitation at this latitude tends to be stronger during boreal summer (June–August, JJA) compared to winter (Figure 3e,b). Note that there are noticeable differences in westward-moving wave phase speeds during December–February (DJF) and JJA; DJF westward waves propagate more slowly than those in JJA. This is particularly noticeable for WMRG waves (Figure 3c,f) and may be explained by differences in the DJF and JJA zonal mean state, which can Doppler-shift equatorial waves (Yang and Hoskins, 2016). There is evidence in the westward-propagating waves, particularly WMRG during JJA (Figure 4f), of an eastward group velocity, as would be expected from theory. These results suggest that rainfall in SE Asia may be linked to all three equatorial waves in both summer and winter. The relationship is investigated further by examining mean rainfall changes over the full region during high-amplitude wave days in boreal winter and summer (Figures 4 and 5).

Low-level convergence associated with high-amplitude Kelvin waves over 100–105°E and 110–115°E during DJF coincide with significantly increased mean precipitation, relative to the climatological seasonal mean, over Peninsular Malaysia, East Malaysia and regions of Indonesia (Figure 4a,b). For wave convergence over 100–105°E, precipitation increases occur in Peninsular Malaysia, Sumatra, and the west coast of Borneo. As the Kelvin waves propagate through the region, increased precipitation occurs in west Borneo, coincident with the location of Kelvin wave convergence (Figure 4b). As the Kelvin wave propagates further eastward, precipitation in Sulawesi is also increased (Figure 4c). Precipitation anomalies are typically $4 - 8\,\mathrm{mm} \cdot \mathrm{day}^{-1}$. Comparing with the seasonal climatology in Figure 1a these anomalies are approximately 50% of the climatological rainfall in most regions (climatology is up to $12\,\mathrm{mm} \cdot \mathrm{day}^{-1}$ in most regions). There is also suppressed precipitation preceding and following the wave. This would be coincident with the low-level wave divergence (also seen in Figure 3), though this is not always visible in the line contours on the figures since they are composited on high-amplitude wave convergence days.

Convergence in the Northern Hemisphere associated with WMRG waves during winter months is also linked to significantly increased mean precipitation over Peninsular Malaysia, particularly the east coast, with composite precipitation increases of approximately $10\,\mathrm{mm} \cdot \mathrm{day}^{-1}$ (Figure 4g), a comparable magnitude to the climatological

precipitation in the region (Figure 1a). Figure 4g–i show that anomalous winds during high-amplitude wave days do not closely resemble the theoretical wave structure (Figure 2), though there are southerly winds on the Equator during positive WMRG phase (convergence in Northern Hemisphere) and northerly winds during the negative phase (convergence in Southern Hemisphere). The discrepancy suggests that waves are preferentially embedded in some other large-scale structure such as the Madden–Julian Oscillation or El Niño–Southern Oscillation. R1 wave activity can also be linked to smaller increases in mean precipitation in Peninsular Malaysia (Figure 4d). As the waves propagate over Indonesia, there is reduced precipitation along the Equator during high-amplitude R1 and WMRG waves in both seasons (Figures 4e,k and 5e,f,h,i,l). In the boreal summer months similar increases in precipitation are associated with Kelvin waves (Figure 5a–c). There is also increased precipitation over Java during WMRG waves when convergence is located in the Southern Hemisphere (Figure 5j).

A striking result is the comparatively large increases in Philippines mean rainfall linked to high-amplitude R1 and WMRG waves over 120–125°E, also shown to a slightly lesser extent in DJF (Figure 4f,i and 5f,i). A reason for the link between R1 cyclonic winds and rainfall increases is the occurrence of tropical cyclones that project onto the R1 wave structure. Previous studies have found linkages between tropical cyclones and equatorial wave identification using outgoing long-wave radiation (OLR) (Schreck *et al.*, 2011; 2012; Aiyyer *et al.*, 2012). This means that many of the days with high-amplitude wave activity are also those during which a tropical cyclone occurs in the region. This is also the case for the WMRG wave days. Indeed, 89% of the R1 JJA days (86% for WMRG wave days; see Table 1) that R1 cyclonic winds (WMRG convergence) occur over 120–125°E are also days that tropical cyclones occur between 110–135°E and 5–25°N. If these days are removed from the composite analysis then the increased mean rainfall signal during JJA is no longer significant. For this reason the JJA precipitation changes over the Philippines will not be addressed in further detail in the remainder of this study, since they are likely simply a result of tropical cyclones, not wave activity. For DJF, tropical cyclones occur less often on the same days; 38% of R1 days and 29% of WMRG days. Some precipitation increases remain for non-tropical cyclone days so DJF Philippines rainfall will be examined more closely in Section 3.2.

3.1.2 | Extreme SE Asia rainfall

Figure 6 shows the change in the likelihood of heavy precipitation (calculated as described in Section 2) for
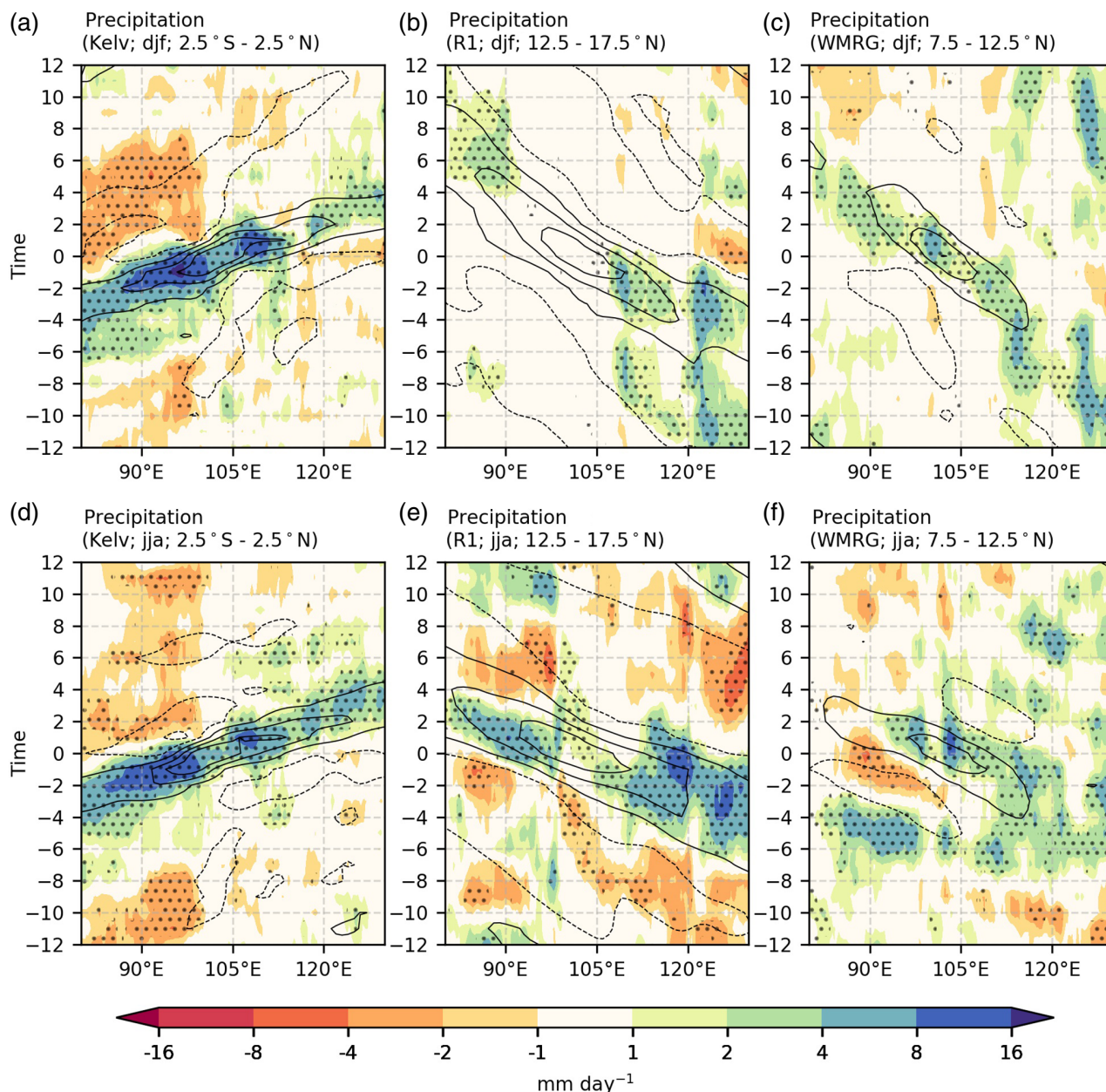
FIGURE 3 Hovmüller of composite anomaly in latitude-averaged TRMM precipitation from seasonal mean (wave composite minus all days 1998–2016 seasonal mean) for days preceding and following high-amplitude waves over 100–105°E for (a) Kelvin wave in DJF, (b) R1 wave in DJF, (c) WMRG wave in DJF, (d) Kelvin wave in JJA, (e) R1 wave in JJA, and (f) WMRG in JJA. The latitude-averaging bounds are given on the figures and were chosen to coincide with the meridional peak of wave activity. Stippling indicates significant difference from the 1998–2016 seasonal mean at the 95% confidence level, based on Student's t-test. Line contours are the composite 850 hPa convergence for Kelvin (latitude 0°) and WMRG (latitude 10°N) waves with intervals beginning -1.25×10^{-6} s^{-1} increasing by 5×10^{-7} s^{-1}. Line contours for R1 waves indicate vorticity (latitude 5°N) in intervals beginning -0.25×10^{-6} s^{-1} increasing by 1×10^{-7} s^{-1}. Solid lines indicate convergence/positive vorticity at 850 hPa, dashed lines indicate divergence/negative vorticity at 850 hPa

some specific high-amplitude wave cases where mean precipitation anomalies are largest. The chance of extreme precipitation is increased on days when there is high-amplitude wave activity in the region relative to all days in 1998–2016, consistent with the increases in mean precipitation previously discussed (Figure 6). During DJF, extreme precipitation, defined as rainfall exceeding the

95th percentile of climatological rainfall for 1998–2016 at each grid point, is at least twice as likely to occur (exceeding 10% in Figure 6, since there is a 5% chance for extreme precipitation for all days in 1998–2016) over large regions of Malaysia on days when there is convergence associated with a high-amplitude Kelvin wave over 100–105°E longitude (Figure 6a). Similarly, extreme rainfall is at
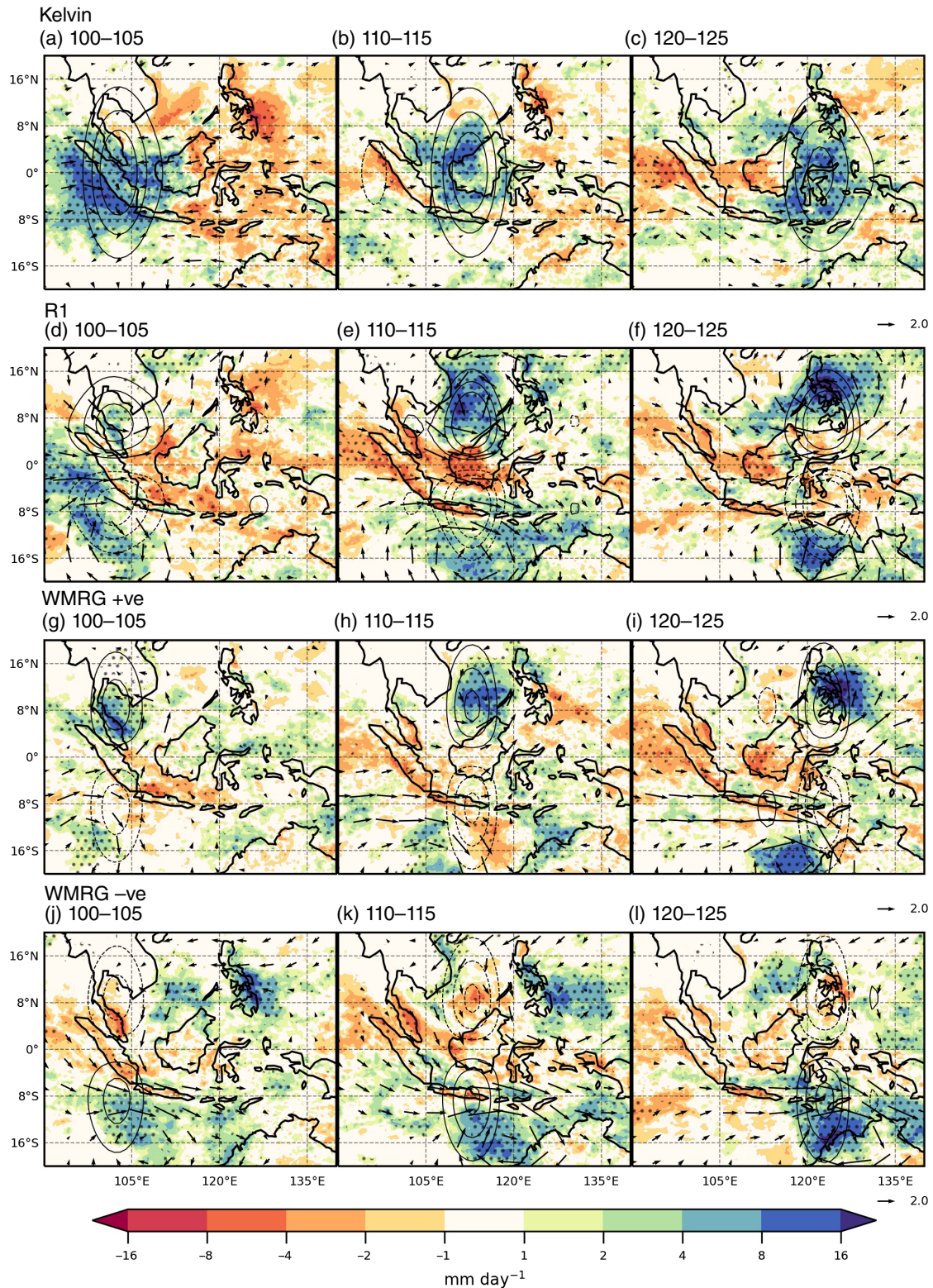
FIGURE 4 (a–l) Composites of anomaly in DJF TRMM precipitation from seasonal mean (wave composite minus all days seasonal mean) for days with high-amplitude wave convergence (for Kelvin and WMRG panes) or vorticity (for R1 panes) at 850 hPa at varying longitude (°E) ranges. Stippling indicates regions where composite precipitation is significantly different from the 1998–2016 seasonal mean at the 95% confidence level based on Student's t-test. Line contours show the composite 850 hPa convergence or vorticity of the relevant wave field with intervals of 5 and 1×10^{-7} s^{-1} respectively. Solid lines indicate convergence/positive vorticity at 850 hPa, dashed lines indicate divergence/negative vorticity at 850 hPa. Vectors show ERA-Interim composite of anomaly in 850 hPa winds
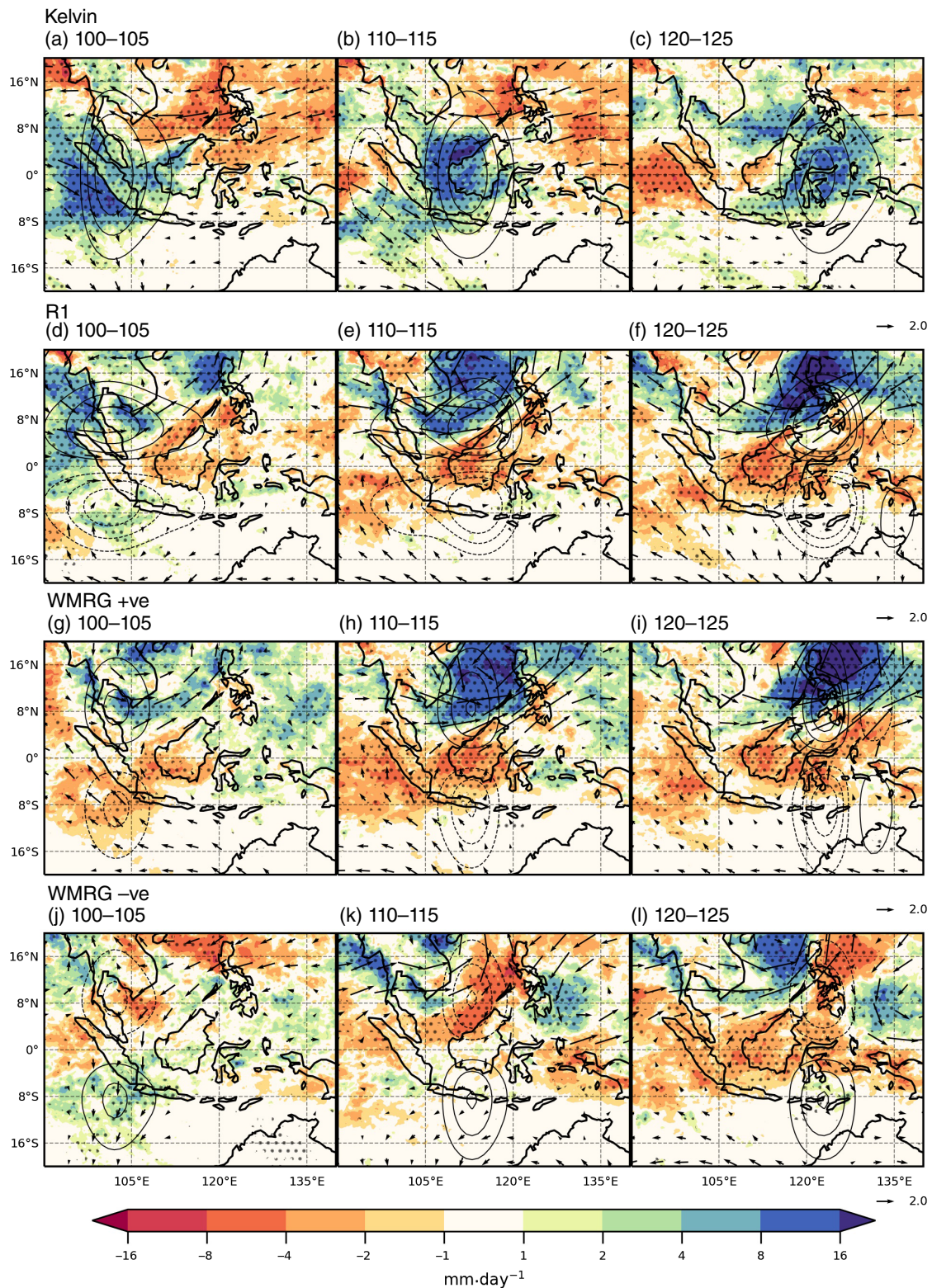
FIGURE 5 (a–l) As in Figure 4 but during JJA

least twice as likely to occur over Peninsular Malaysia, Cambodia and Vietnam during a high-amplitude WMRG wave in DJF (Figure 6e). A high-amplitude Kelvin wave occurring further east, over East Malaysia and Indonesia, can be linked to an increase in the likelihood of extreme precipitation of 2–3 times in those regions, as well as the south of the Philippines (values up to 15% in Figure 6b,c). During high-amplitude R1 wave events over Peninsular

Malaysia extreme precipitation is also at least twice as likely to occur (Figure 6d). Extreme precipitation in some coastal regions of Java and Sumatra is at least twice as likely to occur during boreal summer when WMRG wave convergence occurs over the region (Figure 6f).

3.1.3 | Rainfall on wet days

Examination of changes in the likelihood of wet days (days when rainfall exceeds $1\,\mathrm{mm\cdot day^{-1}}$) and the mean amount of rainfall on wet days during high-amplitude waves provides an idea of whether rainfall increases during equatorial waves are caused by increased frequency of rainfall or an increase in rainfall intensity. It is found that during high-amplitude waves there is both an increase in the frequency of wet days (Figure 7), as well as an increase in the amount of rainfall that occurs on wet days (Figure 8), compared to the climatology. Similar results were found when examining the change in the ratio of the likelihood of extreme rainfall to the likelihood of a wet day, demonstrating increases in the likelihood of extreme precipitation on wet days during high-amplitude waves (not shown in figures). Therefore, increased rainfall during high-amplitude waves arises as a result of both more frequent rainfall and more intense rainfall. Figures suggest that increased rainfall intensity dominates the rainfall response for R1 and WMRG waves (Figure 8d–f), as opposed to similar contributions from both rainfall frequency and intensity for Kelvin wave days (Figures 7a–c and 8a–c).

3.2 | Equatorial waves and regional rainfall percentiles

To summarise the statistical relationship between equatorial waves and rainfall in SE Asia, the percentiles of precipitation for all land grid points in specified regions (see boxed regions in Figure 1e) for all days and for high-amplitude wave days at various longitude ranges in SE Asia are shown in Figure 9 for Malaysia, Figure 10 for Indonesia and Figure 11 for the Philippines. Percentiles are displayed as box plots with upper and lower bounds corresponding to the 95th and 5th percentiles respectively. The climatological values (percentiles calculated using all days in 1998–2016) are shown by dashed horizontal lines. Only the land points are used in the calculation of the percentiles. Note that percentiles can be equal to zero, particularly in drier regions or times of year. Because of this the lower whiskers (5th percentile), lower box bounds (25th percentile) or median line (50th percentile) etc. may not always be visible in Figures 9–11. The climatology

percentile lines are labelled indicating which percentile they correspond to. Labels are only displayed for percentiles not equal to zero, providing an indicator for how much rainfall each region has.

3.2.1 | Malaysia

Rainfall in Peninsular Malaysia during winter (defined as longitude 100–105°E and latitude 2.5–7.5°N; box PM in Figure 1e) is affected by all three equatorial waves (Figure 9a). Convergence associated with Kelvin and WMRG waves over the same longitude range (100–105°E) coincide with an increase in the amount of rainfall compared to the climatological percentiles, resulting in a more positively skewed rainfall distribution. The 95th percentile is increased by 42% and 95% for Kelvin and WMRG waves respectively. For both cases, precipitation increases are located with the peak of the wave convergence (i.e. Figure 4a,g). The Kelvin wave is also linked to smaller increases in summer rainfall in Peninsular Malaysia (also shown in Figure 5a), but other waves have little link to changes in summer rainfall in this region (Figure 9c).

Kelvin and WMRG waves can also be linked to suppressed precipitation in Peninsular Malaysia, that is when the Kelvin wave convergence is located at 90–95°E, or the positive phase of the WMRG wave is located east of 110°E. This is likely to be a result of divergence that follows and precedes wave convergence, suppressing precipitation. Indeed, when the negative phase of the WMRG wave, where divergence is in the Northern Hemisphere, is over 100–105°E there is also suppressed precipitation (see also Figure 4j).

Increased East Malaysia (longitude 110–120°E, latitude 2.5–7.5°N; box EM in Figure 1e) rainfall can also be associated with high-amplitude Kelvin waves over the region (Figure 9b,d; also Figures 4b and 5b), though the increases are less than those in Peninsular Malaysia (95th percentile increased by up to 20%). Increases in DJF East Malaysia rainfall are also observed on high-amplitude R1 and WMRG wave days, but are relatively small (Figure 9b). The 95th percentile is increased by up to 25% and 15% on high-amplitude R1 and WMRG days respectively. Rainfall during JJA in East Malaysia is less changed during high-amplitude waves than in DJF; however, there is still slightly increased precipitation on high-amplitude Kelvin wave days (Figure 9d).

3.2.2 | Indonesia

Changes in Indonesia rainfall distributions are most strongly associated with Kelvin wave convergence
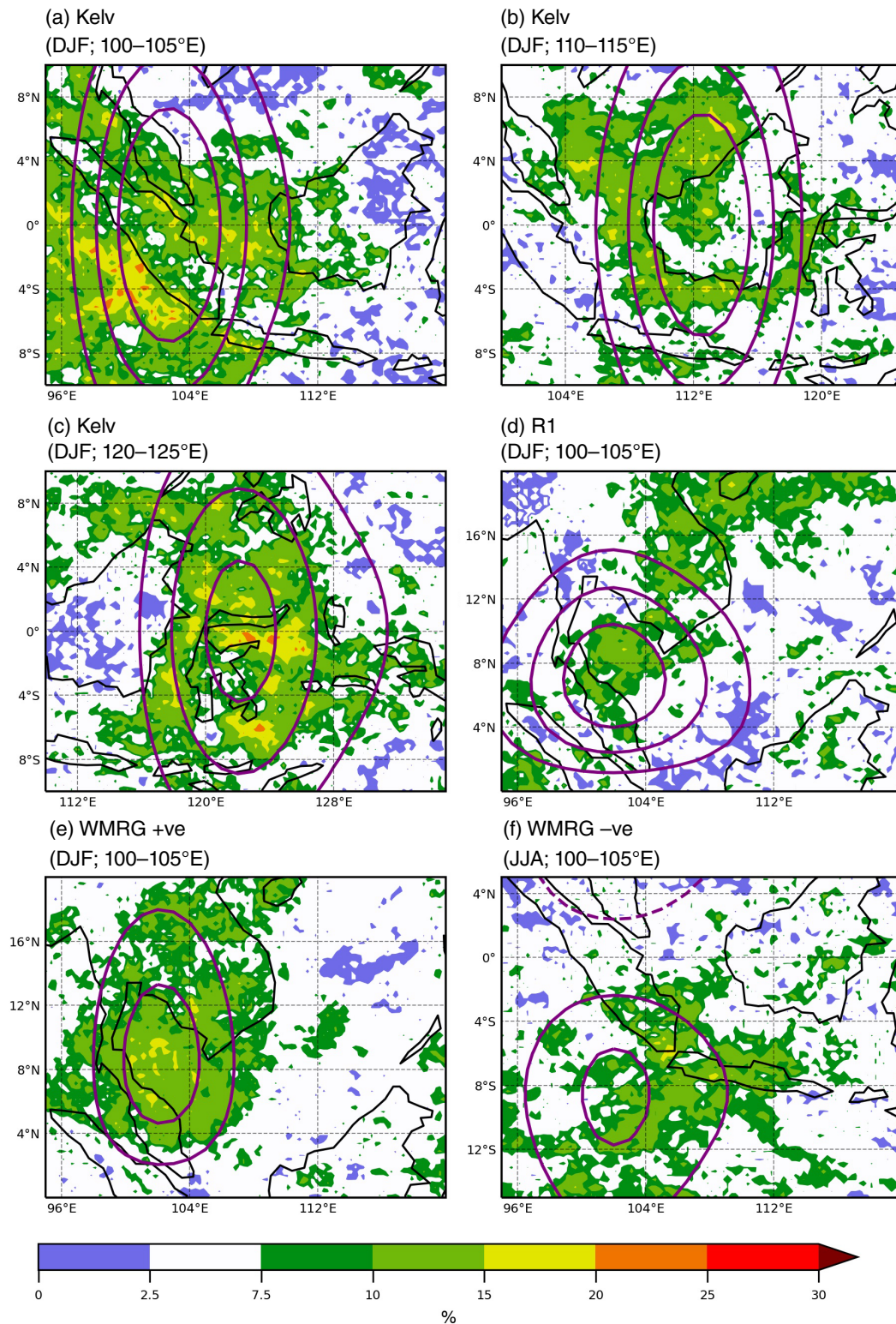
FIGURE 6 Likelihood of extreme precipitation (exceeding 95th percentile of precipitation for 1998–2016) during days with high-amplitude wave activity at 850 hPa (the 95th percentile of wave wind convergence or vorticity). Cases shown are (a) Kelvin wave at 100–105°E in DJF, (b) Kelvin wave at 110–115°E in DJF, (c) Kelvin wave at 120–125°E in DJF, (d) R1 wave at 100–105°E in DJF, (e) positive phase WMRG wave at 100–105°E in DJF, and (f) negative phase WMRG wave at 100–105°E during JJA. A value of 5% indicates no difference from the climatology. Line contours show the composite 850 hPa convergence or vorticity of the relevant wave field with intervals of 5 and 1×10^{-7} s^{-1} respectively. Solid purple lines indicate convergence/positive vorticity at 850 hPa, dashed purple lines indicate divergence/negative vorticity at 850 hPa
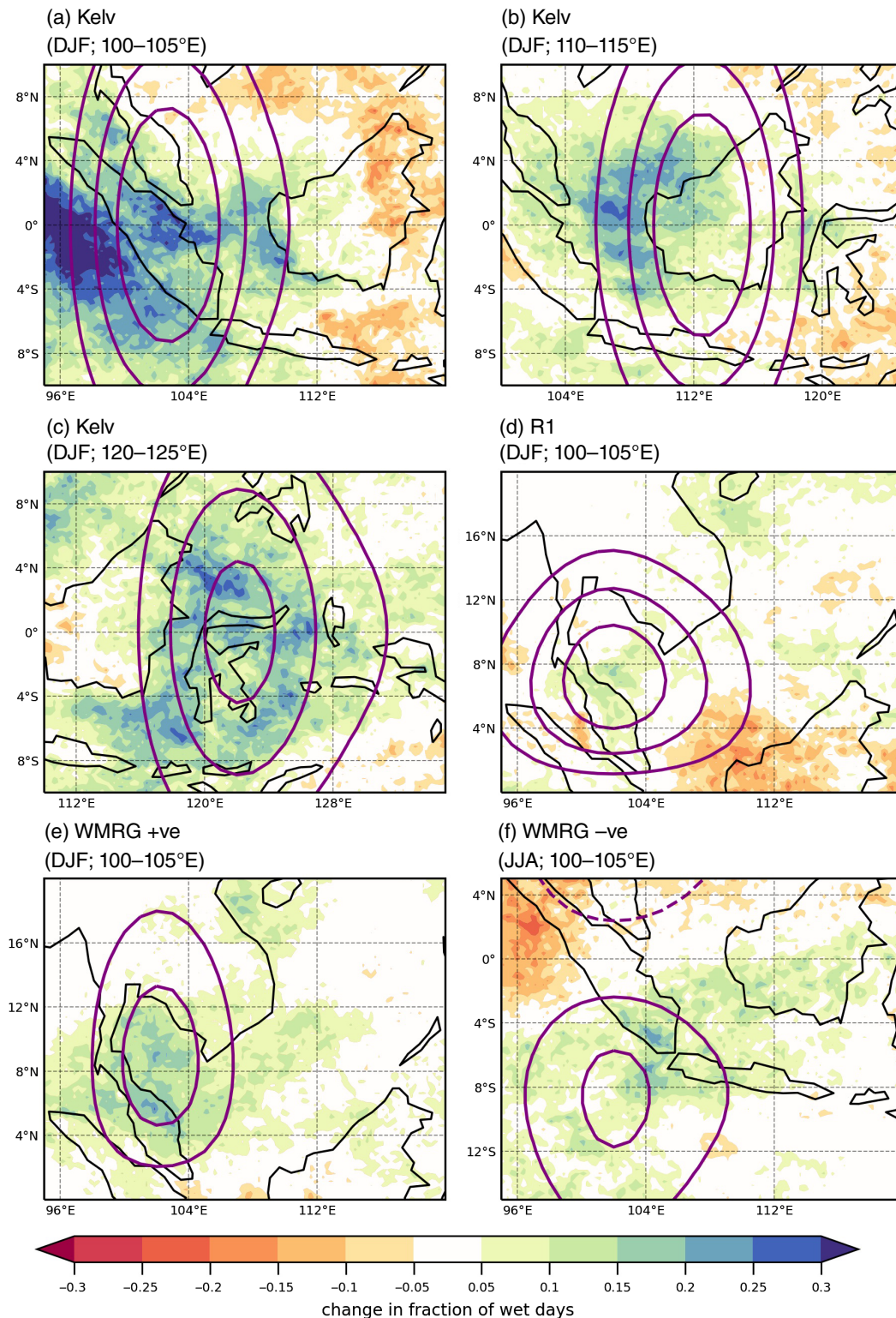
FIGURE 7 (a–f) As in Figure 6 but for the change in the fraction of days with rainfall greater than 1 mm·day^{-1}

(Figures 4,5 and 10). The precipitation distribution in the west region of Indonesia covering Sumatra (longitude 100–105°E, latitude 10°S–2.5°N; box WI in Figure 1e) is more positively skewed when high-amplitude Kelvin waves are over longitude range 100–105°E (the second

bars in the sets of four in Figure 10; DJF 50th, 75th and 95th percentiles increased by 335%, 97% and 44% respectively). As Kelvin waves propagate eastward other regions of Indonesia experience increased rainfall; increased JJA precipitation is observed over the region containing

FIGURE 8 (a–f) As in Figure 6 but for the change in mean rainfall on days with rainfall greater than 1 mm·day^{-1}. Stippling indicates a significant change at 95% confidence level based on Student's *t*-test
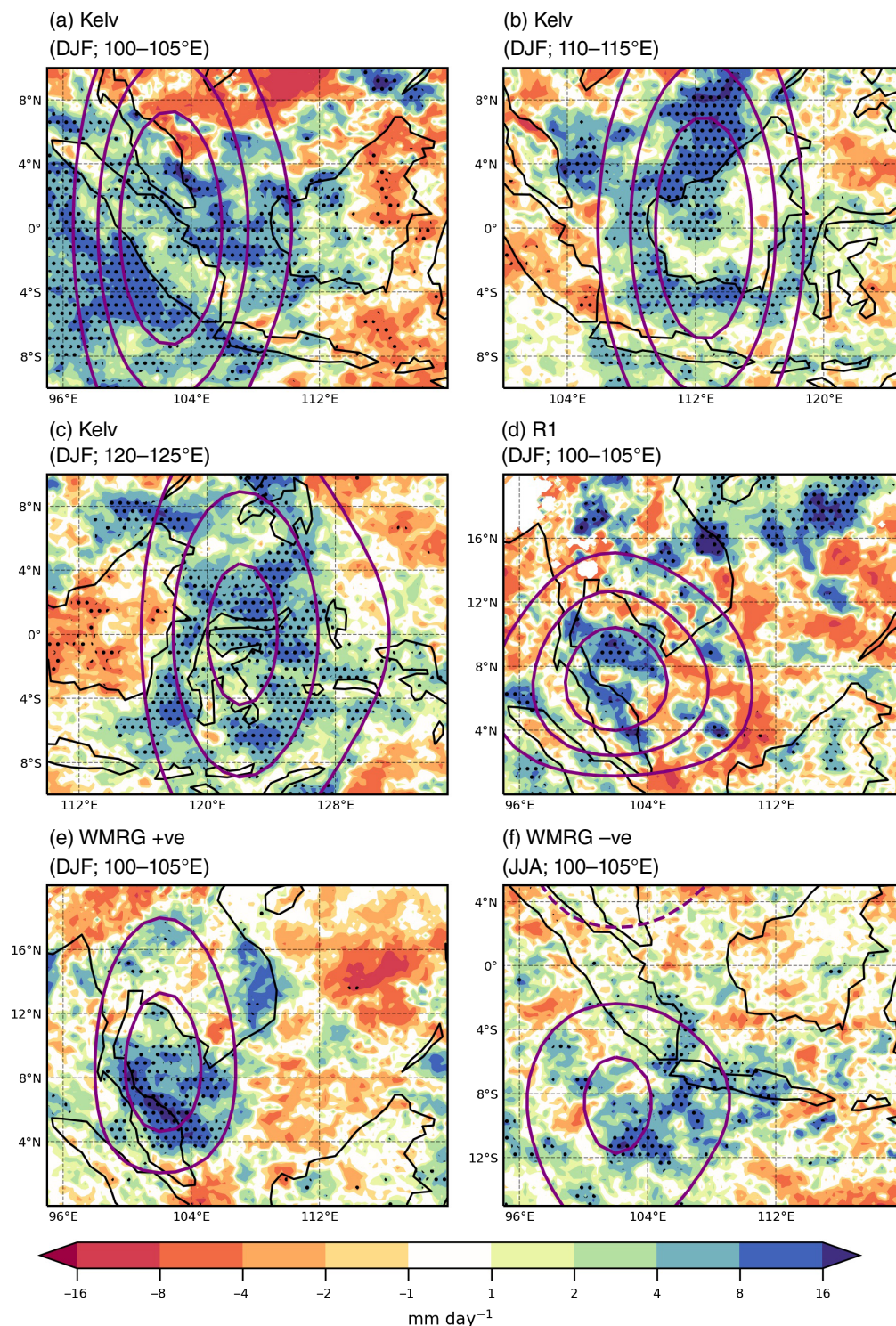
Java (longitude 105–117.5°E, latitude 10–5°S; box SI in Figure 1e) and the regions covering parts of Kalimantan and Sulawesi (longitude 107.5–118°E and 118–125°E, latitude 5°S–2.5°N; boxes NI and EI in Figure 1e) during high-amplitude Kelvin waves east of 100°E (Figure 10).

R1 and WMRG waves are less strongly linked to the precipitation distribution over Indonesia, though high-amplitude R1 and WMRG waves over longitudes east

of 110°E do coincide with suppressed JJA precipitation in all Indonesia regions (Figure 10e–h). This is consistent with the structure of these two waves, since divergence associated with the waves will be present over this part of Indonesia as they propagate through the region (Figure 5). The negative phase of the WMRG wave, where wave convergence is in the Southern Hemisphere, can be linked to increased JJA precipitation in Java (Figure 10f). Rainfall
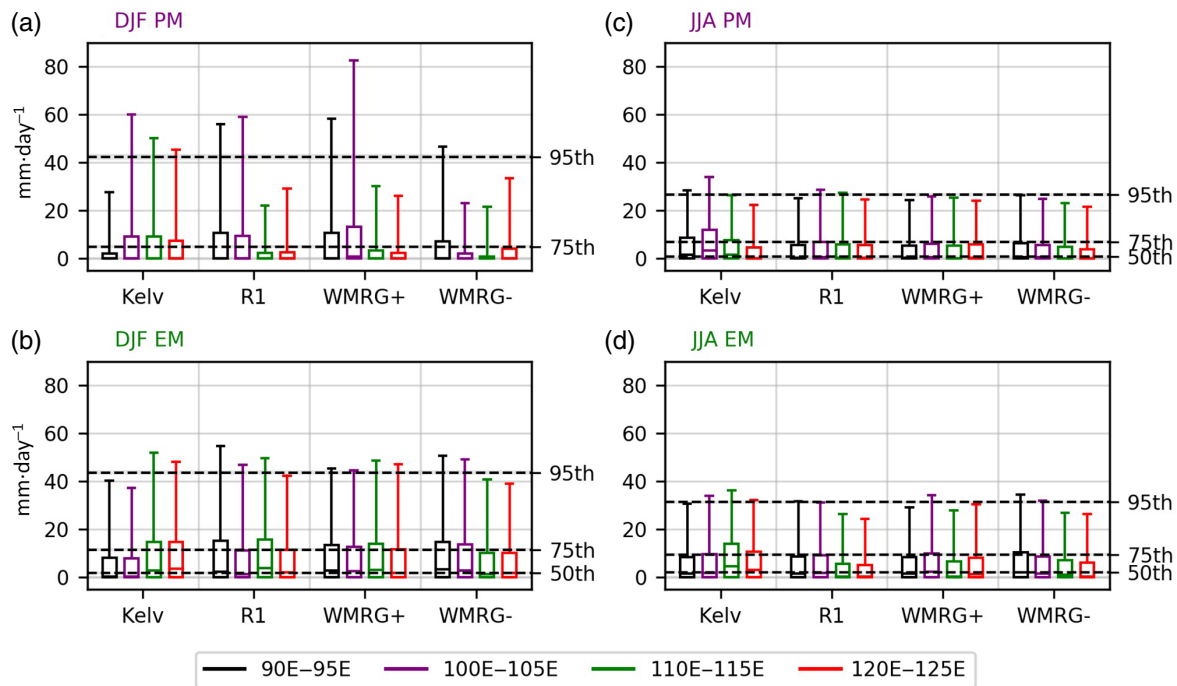
FIGURE 9 Boxplots of percentiles of TRMM rainfall over land in Malaysia boxed regions for all days (dashed lines) and high-amplitude wave activity days for waves over 90–95°E (first bars), 100–105°E (second bars), 110–115°E (third bars), and 120–125°E (fourth bars). Percentiles are calculated for (a) DJF PM, (b) DJF EM, (c) JJA PM and (d) JJA EM. The PM and EM boxed regions are shown in Figure 1e. Values shown by the boxplots are the 5th (lower whisker), 25th (lower box bound), 50th (median; middle box line), 75th (upper box bound) and 95th (upper whisker) percentiles. Typically, at least the 5th and 25th percentiles are zero; only non-zero percentiles are visible on figures. Titles are coloured based on the closest wave longitudinal range to the region

during boreal winter months in Indonesia is less affected by high-amplitude R1 and WMRG waves (Figure 10a–d).

3.2.3 | The Philippines and the role of tropical cyclones

Dramatic increases in DJF precipitation in both regions of the Philippines are associated with high-amplitude R1 and WMRG waves (Figures 4f,i, 5f,i and 11a,b). The north Philippines (longitude 120–130°E, latitude 12.5–20°N; box NP in Figure 1e) rainfall is increased more during high-amplitude R1 waves in the region 120–125°E, compared to the south Philippines (SP; Figure 11a,b). The 95th percentile of NP and SP precipitation is increased by 128% and 332% on these days respectively. As previously mentioned, tropical cyclones also occur in the region on 38% of R1 DJF composite days for high-amplitude waves in 120–125°E and on 29% of WMRG composite days (Table 1). Therefore, analysis can be carried out for days during which a high-amplitude wave and a tropical cyclone occur simultaneously, and for days when only a high-amplitude wave occurs. This allows for an idea of the extent to which tropical cyclones impact on the observed precipitation changes during high-amplitude waves.

Precipitation percentiles of days on which a tropical cyclone and high-amplitude wave occur together over SP and NP are shown in Figure 9c,d. The changes in the rainfall are comparable to those for all days (Figure 11a,b) such that there are large increases in the higher percentiles of precipitation during high-amplitude R1 and WMRG wave days over 120–125°E, suggesting that tropical cyclones do indeed play a role in the increased precipitation observed for all wave days. However, examining days with a high-amplitude wave and no tropical cyclone in the vicinity (Figure 11e,f) suggests that wave activity still influences Philippines rainfall even in the absence of tropical cyclones. Both NP and SP regions show more positively skewed rainfall distributions when high-amplitude waves occur over regions to the east of 110°E.

For the south Philippines in particular, percentiles associated with the high-amplitude R1 and WMRG waves over 120–125°E on non-tropical cyclone days are around 60% of the scale of those for all days (Figure 11e), and the likelihood of extreme rainfall is still increased in some regions by up to three times (not shown in figures), suggesting high-amplitude waves may still play a role in south Philippines rainfall. Note that high-amplitude negative WMRG waves over 100–105°E are also linked to increased Philippines rainfall, despite this being classified
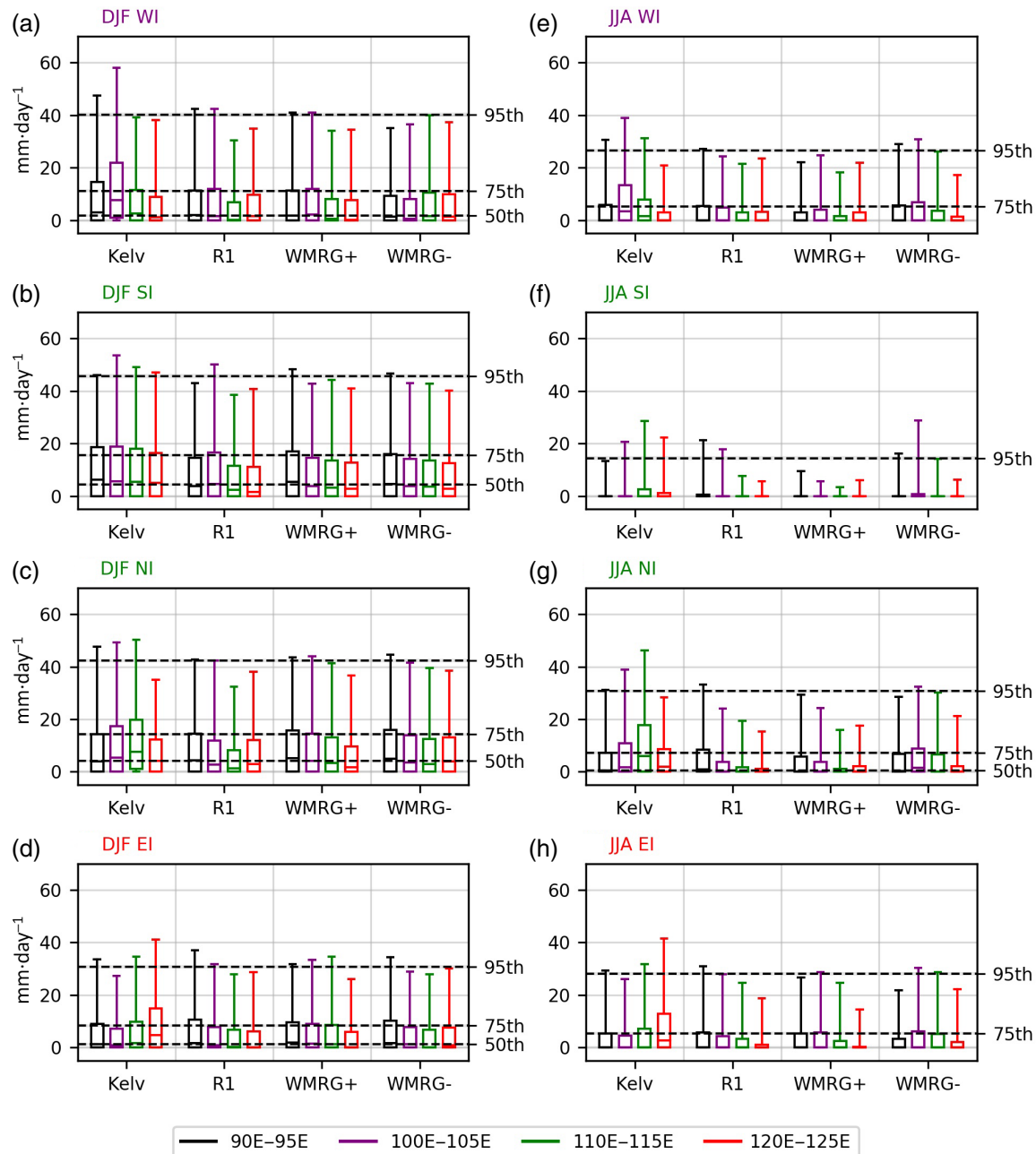
FIGURE 10   (a–h) As in Figure 9 but for Indonesia boxed regions, WI, SI, NI and EI, shown in Figure 1e

as strong convergence in the Southern Hemisphere, and therefore divergence in the Northern Hemisphere. This is because these days will likely be followed or preceded by strong Northern Hemisphere wave convergence, hence there is increased rainfall when the strong Southern Hemisphere convergence is 20° west of the longitude range of the Philippines boxes. Non-tropical cyclone wave days have less influence on rainfall for the north Philippines, and it seems that changes in this region associated with high-amplitude waves at 120–125°E are largely dominated by tropical cyclone days (Figure 11d,f).

4 | SUMMARY

This study examines the link between high-amplitude equatorial waves and winter and summer SE Asia rainfall means and extremes. All three equatorial waves examined, Kelvin, R1 and WMRG, can be linked to changes in the amount of rainfall in SE Asia, with relationships varying depending on the wave, region or season in question. Increased rainfall manifests both in increased mean rainfall and increased probability of occurrence of heavy rainfall on days when high-amplitude waves occur. Rainfall
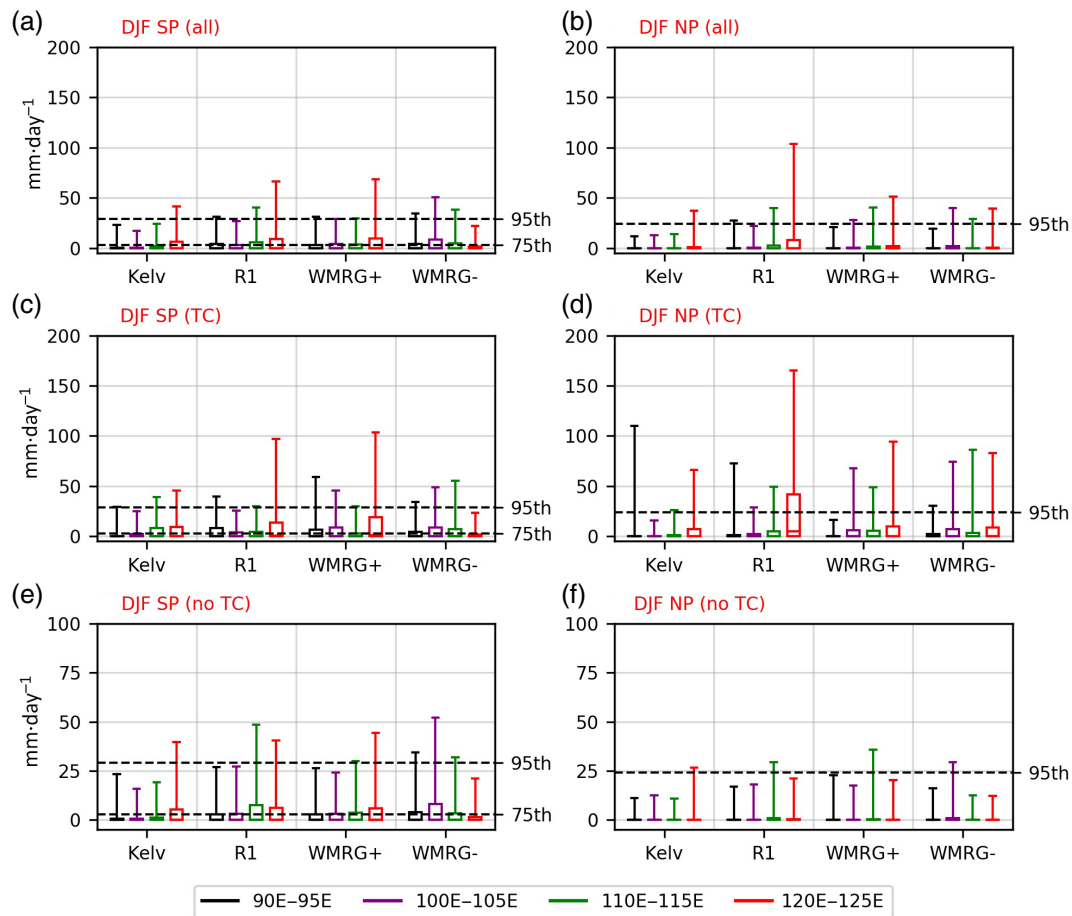
FIGURE 11 As in Figure 9 but for Philippines regions (a) SP and (b) NP for all DJF days. (c,d) Percentiles calculated for only days in (a,b) during which a tropical cyclone is in the vicinity off the Philippines. (e,f) Percentiles calculated for only days in (a,b) during which a tropical cyclone is not in the vicinity. Tropical cyclones are counted if they occur in longitude range 110–135°E and latitude range 5–25°N

increases occur as a result of both increased frequency of rainfall and increased rainfall intensity.

For Indonesia, the largest increases in rainfall are mainly associated with high-amplitude Kelvin waves; the meridional structure of the wave means that wave convergence covers most of Indonesia and the results are consistent with previous studies that find tropical convection propagates in phase with the low-level wave convergence (e.g. Wheeler *et al.*, 2000; Yang *et al.*, 2003; Kiladis *et al.*, 2009; Lubis and Jacobi, 2013). In boreal summer months the negative phase of the WMRG wave, when WMRG convergence is in the Southern Hemisphere, is also linked to increased rainfall over Java, similarly associated with the peak of WMRG wave low-level convergence.

For Malaysia all three waves play a role during DJF, particularly for Peninsular Malaysia. The wave with the most impact is WMRG; high-amplitude WMRG wave days have relatively large increases in mean and extreme precipitation amounts, and increases in the likelihood of heavy rainfall are collocated with WMRG wave convergence. Additional analysis (not shown in figures) finds that there

is no significant link between WMRG wave occurrence in this region and simultaneous cold surges or tropical cyclones, ruling out these as possible reasons for this increase in precipitation. In fact, composite anomalous winds on these days show southwesterly winds to the east of Peninsular Malaysia (Figure 4g), opposite to the response associated with cold surges. Again, the location of wave convergence and anomalous rainfall together is supported by previous studies (e.g. Wheeler *et al.*, 2000; Yang *et al.*, 2003; 2007a; 2007b; Kiladis *et al.*, 2009; Lubis and Jacobi, 2013).

Increases in Philippines rainfall are mostly associated with R1 and WMRG waves. In JJA this is entirely attributable to tropical cyclones occurring on the same days (not shown in figures), since tropical cyclones may project onto the R1 wave structure, or develop embedded within R1 wave structures (Schreck *et al.*, 2011; 2012; Aiyyer *et al.*, 2012). For DJF the rainfall increase is not entirely due to the role of tropical cyclones. Removing tropical cyclone days from analysis still results in significant increases in extreme Philippines precipitation

associated with R1 and WMRG waves. On non-tropical cyclone wave days it is found that, unlike tropical cyclone days, cyclonic winds associated with the wave over 110–115°E have a larger impact on Philippines rainfall (Figure 11e,f). By the theoretical structure of R1 (Figure 2), wave convergence is located to the east of positive vorticity, and so this result may suggest that increased Philippines rainfall is associated with R1 wave convergence (Figure 4e).

This study examines the statistical relationship between heavy SE Asia precipitation and high-amplitude equatorial waves and finds strong evidence for the role of tropical waves on the likelihood of heavy rainfall. A key result is that extreme precipitation is shown to be as much as three times more likely to occur in regions of SE Asia on days when a high-amplitude wave is occurring. We have explored the possible impact of cold surges and tropical cyclones on the statistical analysis and have found that tropical cyclones play a role in the observed relationships of equatorial waves and summer Philippines rainfall. This may be a result of tropical cyclones projecting on R1 and WMRG structures or that tropical cyclones develop within larger-scale R1 and WMRG structures. Rainfall anomalies associated with high-amplitude waves in other regions and seasons were not directly related to tropical cyclones or cold surges.

This study focusses on daily rainfall; however, it is entirely possible that the results presented here are also indicative of the role of equatorial waves in modulating the rainfall diurnal cycle (e.g. Vincent *et al.*, 2016). Examination of equatorial waves and the timing and duration of rainfall is undoubtedly a significant area of future research to gain further insight into the observed relationship between equatorial waves and extreme precipitation.

The results and analysis detailed here forms a basis for future comparison to weather extremes in SE Asia in forecast models, and will enable examination of the shortcomings of models in the representation of equatorial waves and their relationships to high-impact weather. These results indicate that equatorial waves may provide an important source of predictability for high-impact weather in SE Asia and it is crucial for numerical weather prediction models to be able to predict both the behaviour of equatorial waves and their impact on precipitation.

ACKNOWLEDGEMENTS

ORCID

Samantha Ferrett https://orcid.org/0000-0003-4726-847X
Gui-Ying Yang https://orcid.org/0000-0001-7450-3477
Steven J. Woolnough https://orcid.org/0000-0003-0500-8514
John Methven https://orcid.org/0000-0002-7636-6872
Christopher E. Holloway https://orcid.org/0000-0001-9903-8989

REFERENCES

Aiyyer, A., Mekonnen, A., and C.J.Schreck, C.J. (2012) Projection of Tropical Cyclones on Wavenumber–Frequency-Filtered Equatorial Waves. *J. Climate*, 25, 3653–3658, https://doi.org/10.1175/JCLI-D-11-00451.1

Barcikowska, M., Feser, F. and Von Storch, H. (2012) Usability of best track data in climate statistics in the western North Pacific. *Monthly Weather Review*, 140, 2818–2830.

Birch, C.E., Webster, S., Peatman, S.C., Parker, D.J., Matthews, A., Li, Y. and Hassim, M.E.E. (2016) Scale interactions between the MJO and the western Maritime Continent. *Journal of Climate*, 29, 2471–2492.

Chang, C.-P., Harr, P.A. and Chen, H.-J. (2005b) Synoptic disturbances over the equatorial South China Sea and western Maritime Continent during boreal winter. *Monthly Weather Review*, 133, 489–503.

Chang, C.-P., Lu, M.-M. and Lim, H. (2016) Monsoon convection in the Maritime Continent: interaction of large-scale motion and complex terrain. *Multiscale Convection-Coupled Systems in the Tropics: A tribute to Dr Michio Yanai, Meteorological Monograph no. 56. American Meteorological Society*, 6, 1–6.29.

Chang, C.-P., Wang, Z. and Hendon, H. (2006) The Asian winter monsoon. In: *The Asian Monsoon, 89–127*. Berlin, Heidelberg: Springer Praxis Books, Springer.

Chang, C.-P., Wang, Z., McBride, J. and Liu, C.-H. (2005a) Annual cycle of Southeast Asia–Maritime Continent rainfall and the asymmetric monsoon transition. *Journal of Climate*, 18, 287–301.

Dee, D.P., Uppala, S.M., Simmons, A.J., Berrisford, P., Poli, P., Kobayashi, S., Andrae, U., Balmaseda, M.A., Balsamo, G., Bauer, P., Bechtold, P., Beljaars, A.C.M., van de Berg, L., Bidlot, J., Bormann, N., Delsol, C., Dragani, R., Fuentes, M., Geer, A.J., Haimberger, L., Healy, S.B., Hersbach, H., Hólm, E.V., Isaksen, L., Kållberg, P., Köhler, M., Matricardi, M., McNally, A.P., Monge-Sanz, B.M., Morcrette, J.-J., Park, B.-.K., Peubey, C., de Rosnay, P., Tavolato, C., Thépaut, J.-.N. and Vitart, F. (2011) The ERA-interim reanalysis: configuration and performance of the data assimilation system. *Quarterly Journal of the Royal Meteorological Society*, 137, 553–597.

Dias, J. and Kiladis, G.N. (2014) Influence of the basic state zonal flow on convectively coupled equatorial waves. *Geophysical Research Letters*, 41, 6904–6913. https://doi.org/10.1002/2014GL061476.

Gill, A.E. (1980) Some simple solutions for heat-induced tropical circulation. *Quarterly Journal of the Royal Meteorological Society*, 106, 447–462.

Hamada, J.-I., Yamanaka, M.D., Matsumoto, J., Fukao, S., Winarso, P.A. and Sribimawati, T. (2002) Spatial and temporal variations of the rainy season over Indonesia and their link

to ENSO. *Journal of the Meteorological Society of Japan*, 80, 285–310.

Hodges, K., Cobb, A. and Vidale, P.L. (2017) How well are tropical cyclones represented in reanalysis datasets? *Journal of Climate*, 30, 5243–5264.

Huang, P., Chou, C. and Huang, R. (2013) The activity of convectively coupled equatorial waves in CMIP3 global climate models. *Theoretical and Applied Climatology*, 112, 697–711.

Huffman, G.J., Adler, R.F., Bolvin, D.T. and Nelkin, E.J. (2010) The TRMM Multi-satellite Precipitation Analysis (TMPA). In: *Satellite Rainfall Applications for Surface Hydrology*. New York, NY: Springer, pp. 3–22.

Huffman, G.J., Adler, R.F., Bolvin, D.T., Gu, G.J., Nelkin, E.J., Bowman, K.P., Stocker, E. and Wolff, D.B. (2007) The TRMM multi-satellite precipitation analysis: quasi-global, multi-year, combined-sensor precipitation estimates at fine scales. *Journal of Hydrometeorology*, 8, 38–55.

Johnson, S.J., Levine, R.C., Turner, A.G., Martin, G.M., Woolnough, S.J., Schiemann, R., Mizielinski, M.S., Roberts, M.J., Vidale, P.L., Demory, M.-E. and Strachan, J. (2016) The resolution sensitivity of the South Asian monsoon and Indo-Pacific in a global 0.35° AGCM. *Climate Dynamics*, 46, 807–831.

Juneng, L., Tangang, F.T. and Reason, C.J.C. (2007) Numerical case study of an extreme rainfall event during 9–11 December 2004 over the east coast of Peninsular Malaysia. *Meteorology and Atmospheric Physics*, 98, 81–98.

Kiladis, G.N., Wheeler, M.C., Haertel, P.T., Straub, K.H. and Roundy, P.E. (2009) Convectively coupled equatorial waves. *Reviews of Geophysics*, 47(2), RG2003. https://doi.org/10.1029/2008RG000266.

Kim, J. and Alexander, M. (2013) Tropical precipitation variability and convectively coupled equatorial waves on submonthly time scales in reanalyses and TRMM. *Journal of Climate*, 26, 3013–3030.

Knapp, K. R., M. C. Kruk, D. H. Levinson, H. J. Diamond, and C. J. Neumann, (2010) The International Best Track Archive for Climate Stewardship (IBTrACS): unifying tropical cyclone data. *Bulletin of the American Meteorological Society*, 91(3), 363–376.

Li, R.C.Y., Zhou, W., Chan, J.C.L. and Huang, P. (2012) Asymmetric modulation of western North Pacific cyclogenesis by the Madden–Julian Oscillation under ENSO conditions. *Journal of Climate*, 25, 5374–5385.

Liebmann, B., Hendon, H.H. and Glick, J.D. (1994) The relationship between tropical cyclones of the western Pacific and Indian Oceans and the Madden–Julian Oscillation. *Journal of the Meteorological Society of Japan*, 72, 401–411.

Lim, S.Y., Marzin, C., Xavier, P., Chang, C.-P. and Timbal, B. (2017) Impacts of boreal winter monsoon cold surges and the interaction with MJO on Southeast Asia rainfall. *Journal of Climate*, 30, 4267–4281.

Love, B.S., Matthews, A.J. and Lister, G.M.S. (2011) The diurnal cycle of precipitation over the Maritime Continent in a high-resolution atmospheric model. *Quarterly Journal of the Royal Meteorological Society*, 137, 934–947.

Lubis, S. and Jacobi, C. (2013) The modulating influence of convectively coupled equatorial waves (CCEWs) on the variability of tropical precipitation. *International Journal of Climatology*, 35, 1465–1483.

Madden, R.A. and Julian, P.R. (1971) Detection of a 40–50 day oscillation in the zonal wind in the tropical Pacific. *Journal of the Atmospheric Sciences*, 28, 702–708.

Madden, R.A. and Julian, P.R. (1972) Description of global-scale circulation cells in the Tropics with a 40–50 day period. *Journal of the Atmospheric Sciences*, 29, 1109–1123.

Madden, R.A. and Julian, P.R. (1994) Observations of the 40–50-day tropical oscillation – a review. *Monthly Weather Review*, 122, 814–837.

Masunaga, H. (2009) A 9-season TRMM observation of the austral summer MJO and low-frequency equatorial waves. *Journal of the Meteorological Society of Japan*, 87A, 295–315.

Matsuno, T. (1966) Quasi-geostrophic motions in the equatorial area. *Journal of the Meteorological Society of Japan*, 44, 25–43.

Murata, F., Yamanaka, M.D., Hashiguchi, H., Mori, S., Kudsy, M., Sribimawati, T., Suhardi, B. and and Emrizal. (2006) Dry intrusions following eastward-propagating synoptic-scale cloud systems over Sumatera Island. *Journal of the Meteorological Society of Japan Series 2*, 84, 277–294.

Roundy, P.E. and Frank, W.M. (2004) A climatology of waves in the equatorial region. *Journal of the Atmospheric Sciences*, 61, 2105–2132.

Schlueter, A., Fink, A.H., Knippertz, P. and Vogel, P. (2019) A systematic comparison of tropical waves over northern Africa. Part I: Influence on rainfall. *Journal of Climate*, 32, 1501–1523.

Schreck, C. J., Molinari, J., & Mohr, K. I. (2011). Attributing Tropical Cyclogenesis to Equatorial Waves in the Western North Pacific. *Journal of the Atmospheric Sciences*, 68(2), 195–209. https://doi.org/10.1175/2010jas3396.1

Schreck, C. J., Molinari, J., & Aiyyer, A. (2012). A Global View of Equatorial Waves and Tropical Cyclogenesis. *Monthly Weather Review*, 140(3), 774788. https://doi.org/10.1175/mwr-d-11-00110.1

Straub, K.H. and Kiladis, G.N. (2001) Observations of a convectively coupled Kelvin wave in the eastern Pacific ITCZ. *Journal of the Atmospheric Sciences*, 59, 30–53.

Subudhi, A.K. and Landu, K. (2019) Influence of convectively coupled equatorial waves and intra-seasonal oscillations on rainfall extremes over India. *International Journal of Climatology*, 39, 2786–2792.

Takayabu, Y.N. (1994) Large-scale cloud disturbances associated with equatorial waves. *Journal of the Meteorological Society of Japan*, 72, 433–449.

Tangang, F.T.L., Juneng, L., Salimun, E., Vinayachandran, P.N., Seng, Y.K., Reason, C.J.C., Behera, S.K. and Yasunari, T. (2008) On the roles of the northeast cold surge, the Borneo vortex, the Madden–Julian Oscillation, and the Indian Ocean dipole during the extreme 2006/2007 flood in southern peninsular Malaysia. *Geophysical Research Letters*, 35, L14S07. https://doi.org/10.1029/2008GL033429.

Tsuda, T., V. Ratnam, M., Kozu, T. and Mori, S. (2006) Characteristics of 10-day Kelvin wave observed with radiosondes and CHAMP/GPS occultation during the CPEA campaign (April–May, 2004). *Journal of the Meteorological Society of Japan Series 2*, 84A, 277–293.

Van Der Linden, R., Fink, A.H., Pinto, J.G., Phan-Van, T. and Kiladis, G.N. (2016) Modulation of daily rainfall in southern Vietnam by the Madden–Julian oscillation and convectively coupled equatorial waves. *Journal of Climate*, 29, 5801–5820.

Vincent, C.L., Lane, T.P. and Wheeler, M.C. (2016) A local index of Maritime Continent intraseasonal variability based on rain rates over the land and sea. *Geophysical Research Letters*, 43, 9306–9314.

Wheeler, M. and Kiladis, G.N. (1999) Convectively coupled equatorial waves: analysis of clouds and temperature in the wave-number-frequency domain. *Journal of the Atmospheric Sciences*, 56, 374–399.

Wheeler, M., Kiladis, G.N. and Webster, P.J. (2000) Large-scale dynamical fields associated with convectively coupled equatorial waves. *Journal of the Atmospheric Sciences*, 57, 613–640.

Xavier, P., Rahmat, R., Cheong, W.K. and Wallace, E. (2014) Influence of Madden–Julian Oscillation on Southeast Asia rainfall extremes: observations and predictability. *Geophysical Research Letters*, 41, 4406–4412.

Yang, G.Y. and Hoskins, B.J. (2013) ENSO impact on Kelvin waves and associated tropical convection. *Journal of the Atmospheric Sciences*, 70, 3513–3532.

Yang, G.Y. and Hoskins, B.J. (2016) ENSO-related variation of equatorial MRG and Rossby waves and forcing from higher latitudes. *Quarterly Journal of the Royal Meteorological Society*, 142, 2488–2504.

Yang, G.Y., Hoskins, B.J. and Gray, L. (2012) The influence of the QBO on the propagation of equatorial waves into the stratosphere. *Journal of the Atmospheric Sciences*, 69, 2959–2982.

Yang, G.Y., Hoskins, B.J. and Slingo, J.M. (2003) Convectively coupled equatorial waves: a new methodology for identifying wave structures in observational data. *Journal of the Atmospheric Sciences*, 60, 1637–1654.

Yang, G.Y., Hoskins, B.J. and Slingo, J.M. (2007a) Convectively coupled equatorial waves. Part I: Horizontal structure. *Journal of the Atmospheric Sciences*, 64, 3406–3423.

Yang, G.Y., Hoskins, B.J. and Slingo, J.M. (2007b) Convectively coupled equatorial waves. Part II: Zonal propagation. *Journal of the Atmospheric Sciences*, 64, 3424–3437.

Yang, G.Y., Hoskins, B.J. and Slingo, J.M. (2007c) Convectively coupled equatorial waves. Part III: Synthesis structures and extratropical forcing. *Journal of the Atmospheric Sciences*, 64, 3438–3451.

Yang, G.Y., Hoskins, B.J. and Slingo, J.M. (2011) Equatorial waves in opposite QBO phases. *Journal of the Atmospheric Sciences*, 68, 839–862.

Yang, G.Y., Methven, J., Woolnough, S.J., Hodges, K. and Hoskins, B.J. (2018) Linking African easterly wave activity with equatorial waves and the influence of Rossby waves from the Southern Hemisphere. *Journal of the Atmospheric Sciences*, 75, 1783–1809.

Yang, G.Y., Slingo, J. and Hoskins, B.J. (2009) Convectively coupled equatorial waves in high-resolution Hadley Centre climate models. *Journal of Climate*, 22, 1897–1919.

Ying, Y. and Zhang, F. (2017) Practical and intrinsic predictability of multiscale weather and convectively coupled equatorial waves during the active phase of an MJO. *Journal of the Atmospheric Sciences*, 74, 3771–3785.